





# Characterization and closed-loop control of infrared thalamocortical stimulation produces spatially constrained single-unit responses

Brandon S. Coventry <sup>a,b,\*</sup>, Georgia L. Lawlor <sup>a,b</sup>, Christina B. Bagnati<sup>a</sup>, Claudia Krogmeier <sup>c</sup> and Edward L. Bartlett <sup>a,b,d,\*</sup>

<sup>a</sup>Weldon School of Biomedical Engineering, Purdue University, West Lafayette, IN 47907, USA

<sup>b</sup>Center for Implantable Devices and the Institute for Integrative Neuroscience, Purdue University, West Lafayette, IN 47907, USA

<sup>c</sup>Department of Computer Graphics Technology, Purdue University, West Lafayette, IN 47907, USA

<sup>d</sup>Department of Biological Sciences, Purdue University, West Lafayette, IN 47907, USA

\*To whom correspondence should be addressed: Email: [ebartlett@purdue.edu](mailto:ebartlett@purdue.edu) (E.L.B.); Email: [coventry@wisc.edu](mailto:coventry@wisc.edu) (B.S.C.)

Edited By: Rui Reis

## Abstract

Deep brain stimulation (DBS) is a powerful tool for the treatment of circuitopathy-related neurological and psychiatric diseases and disorders such as Parkinson's disease and obsessive-compulsive disorder, as well as a critical research tool for perturbing neural circuits and exploring neuroprostheses. Electrically mediated DBS, however, is limited by the spread of stimulus currents into tissue unrelated to disease course and treatment, potentially causing undesirable patient side effects. In this work, we utilize infrared neural stimulation (INS), an optical neuromodulation technique that uses near to midinfrared light to drive graded excitatory and inhibitory responses in nerves and neurons, to facilitate an optical and spatially constrained DBS paradigm. INS has been shown to provide spatially constrained responses in cortical neurons and, unlike other optical techniques, does not require genetic modification of the neural target. We show that INS produces graded, biophysically relevant single-unit responses with robust information transfer in rat thalamocortical circuits. Importantly, we show that cortical spread of activation from thalamic INS produces more spatially constrained response profiles than conventional electrical stimulation. Owing to observed spatial precision of INS, we used deep reinforcement learning (RL) for closed-loop control of thalamocortical circuits, creating real-time representations of stimulus-response dynamics while driving cortical neurons to precise firing patterns. Our data suggest that INS can serve as a targeted and dynamic stimulation paradigm for both open and closed-loop DBS.

**Keywords:** infrared neural stimulation, deep brain stimulation, closed-Loop DBS, deep reinforcement learning

## Significance Statement

Despite initial clinical successes, electrical deep brain stimulation (DBS) is fraught with off-target current spillover into tissue outside of therapeutic targets, giving rise to patient side effects and the reduction of therapeutic efficacy. In this study, we validate infrared neural stimulation (INS) as a spatially constrained optical DBS paradigm by quantifying dose-response profiles and robust information transfer through INS-driven thalamocortical circuits. We show that INS elicits biophysically relevant responses that are spatially constrained compared to conventional electrical stimulation, potentially reducing off-target side effects. Leveraging the spatial specificity of thalamocortical INS, we used deep reinforcement learning (RL) to close the loop on thalamocortical INS and showed the ability to drive subject-specific thalamocortical circuits to target response states in real-time.

## Introduction

Electrical stimulation of the nervous system has emerged as a potent tool for the treatment and study of a wide variety of neurological diseases (1–5), as well as a key research tool for modulating and mapping neural circuits (6–9). The most prominent of these stimulation paradigms are cochlear implants (CI), which induce sound percepts in individuals with profound hearing loss, and deep brain stimulation (DBS), which has proven

effective in treating movement-related symptoms associated with Parkinson's disease and essential tremor. Additionally, diseases treated by electrical neuromodulation are expanding, with anterior thalamic DBS receiving United States Food and Drug Administration (FDA) approval for the treatment of drug-refractory epilepsy (10) and interior capsule DBS receiving FDA humanitarian device exemption for treatment-resistant obsessive-compulsive disorder (11). DBS is also currently in

**Competing Interest:** B.S.C. and E.L.B. hold a provisional patent on the SpikerNet closed-loop reinforcement learning-based neuromodulation system presented (USPTO: 18/083490). G.L.L., C.B.B., and C.M.K. declare no competing interests.

**Received:** October 19, 2023. **Accepted:** February 7, 2024

© The Author(s) 2024. Published by Oxford University Press on behalf of National Academy of Sciences. This is an Open Access article distributed under the terms of the Creative Commons Attribution-NonCommercial-NoDerivs licence (<https://creativecommons.org/licenses/by-nc-nd/4.0/>), which permits non-commercial reproduction and distribution of the work, in any medium, provided the original work is not altered or transformed in any way, and that the work is properly cited. For commercial re-use, please contact [journals.permissions@oup.com](mailto:journals.permissions@oup.com)

clinical safety and efficacy trials for the treatment of major depressive disorder (3) and Tourette syndrome (1). Peripheral nerve electrical stimulation technologies are also maturing into viable clinical tools, including vagus nerve stimulation for the treatment of epilepsy (12) and carotid sinus stimulation for the treatment of heart disease (2).

Despite initial clinical success, electrical paradigms of neuromodulation are fraught with undesirable current spillover into off-target neural circuits (13–17) leading to undesirable side effects and a reduction in therapeutic efficacy (18–20). The development of focal stimulation strategies is paramount to more effective clinical stimulation and the improvement of patient side-effect profiles. One such tool is infrared neural stimulation (INS), an optical modality that stimulates nerves and neurons using near to midinfrared wavelength (700–2,000 nm) light (21–24). INS has shown spatially specific recruitment of both peripheral nerves (17, 25, 26) and central neurons (23, 24). Importantly, INS does not require genetic manipulation necessary for other optical stimulation methods (27), though at the cost of cell type-specific activation afforded by genetic tools, with INS acting purportedly on intrinsic cell biophysics (28). INS also shows promising safety profiles for translation to human patients (29–31) and has found use in diagnostic targeting of human nerve roots in surgical resection procedures (32). While INS is a promising modality for neuromodulation therapies, progress toward optically based DBS (oDBS) is hindered by a lack of understanding of INS entrainment of thalamocortical and subthalamocortical networks; the understanding of which is necessary for treating “circuitopathies” associated with diseases treated by DBS (33–38). Specifically, there is a dearth of information related to dose-response dependencies of INS laser parameters in circuitual recruitment and the resulting spread of activation across neural circuits.

In this study, we validate INS as a potent oDBS paradigm by quantifying INS dose-response profiles from varying laser parameters, INS driven information transmission across the thalamocortical synapse, and spatial specificity of network INS in the rat auditory thalamocortical model. Our experiments show strong evoked firing rate dependence on applied laser energy with increases in thalamocortical information transfer with increased laser energy. We further show that INS evokes cortical activity that maintains typical thalamocortical response profiles with constrained spread of activation well below the spread of electrical stimulation. Owing to the targeted neural activation of INS, we engineered a closed-loop control approach called SpikerNet, a deep reinforcement learning (RL) based reactive DBS system (39, 40). Closed-loop DBS utilizes feedback from biomarkers of disease to apply stimulation only when needed (41) and has shown advantageous therapeutic efficacy and improved battery life (42). However, the relatively simple control algorithms of conventional closed-loop DBS limit the ability to capture complex dynamics of neural activity related to disease which can cause interference with normal activity, such as interruption of volitional movement (43) which is further exacerbated by large-scale activation from electrical stimulation (44). More complex control methods are advantageous in accounting for brain-wide state changes, such as sleep-wake cycles (45). We, therefore, utilized deep RLs ability to develop statistical mappings of systems in response to state perturbations in order to drive cortical activity to desired firing states.

## Results

In this study, INS as a spatially specific DBS platform was assessed in a chronic rodent implantation preparation ( $n = 7$  animals). In

order to examine the effects of the optrode implantation on auditory pathway neurotransmission, subcortical and thalamocortical function was quantified through comparison of pre and postsurgical electroencephalographic midlatency responses (MLR) ( $n = 6$  animals). Dose-response relationships between applied INS energy and single-unit firing rates were quantified using hierarchical linear regressions, with information theoretic analysis showing INS provides robust information transfer across the thalamocortical synapse. Joint-peristimulus time histogram (JPSTH) analysis was utilized to quantify cortical spread resulting from thalamic INS. Owing to INS spatially constrained activation profiles, a novel RL-based closed-loop control paradigm was designed to drive subject-specific neural dynamic representation and control.

## Implantation of stimulation and recording devices

The auditory pathway has a rich history of neuromodulation, with electrical stimulation of the cochlea resulting in CI, one of the first and most successful clinical neuromodulation devices (46). Other clinical auditory devices include the auditory brainstem and mid-brain implants (47, 48) with electrical neuromodulation across all auditory nuclei (49–51) being investigated for clinical viability. Auditory thalamocortical circuits are particularly suited for neurostimulation because the regional architecture of the auditory thalamus permits stimulation of both core and belt pathways in rodents, primates (52), and humans (53) using a single dorsoventrally oriented electrode. This enables testing stimulation strategies simultaneously in both tonotopic core pathways and higher-order belt pathways, along with the ability to rapidly test circuit function with minimally invasive scalp-evoked auditory potentials (54–56) before and after device implantation. To facilitate understanding of dose-response effects of network function elicited through INS, rats were implanted with fiber optic optrodes into the medial geniculate body (MGB) of the auditory thalamus. The ventral and dorsal divisions of the MGB have primary excitatory afferents to layer 3/4 of auditory cortex (57), while the medial division targets layers 1 and 6 more heavily (Fig. 1A and C) with all MGB subdivisions having at least some projection to primary auditory cortex (58). Sixteen channel planar arrays were implanted into layer 3/4 of primary auditory cortex (Fig. 1A). Postmortem histological analyses confirmed placement of optrodes into the MGB (Fig. 1D and [Supplementary Methods](#)).

Development of INS into a clinically viable neuromodulation system has been limited by a lack of understanding of underlying stimulation mechanisms and stimulus-to-response mappings. A confounding factor is that commercial INS systems are not widely available and are prohibitively expensive or removed from the market by product recalls (59). To facilitate continued INS studies, we developed INSight, a low-cost open source INS and optical stimulation system which uses off-the-shelf components for ease of building and modification. Importantly, INSight can integrate into established recording systems. Materials, build instructions, and calibrations are found in the [Supplementary Material](#) (Figs. S10 and S11) and the INSight Github repository: <https://github.com/bscoventry/INSight>.

## Changes in neural activity due to presence of devices in the brain

Implantation of recording and stimulation devices evokes an injury response and may perturb normal neural function (60, 61). Therefore, we first considered the effect of the presence of stimulation and recording devices on brain activity through auditory

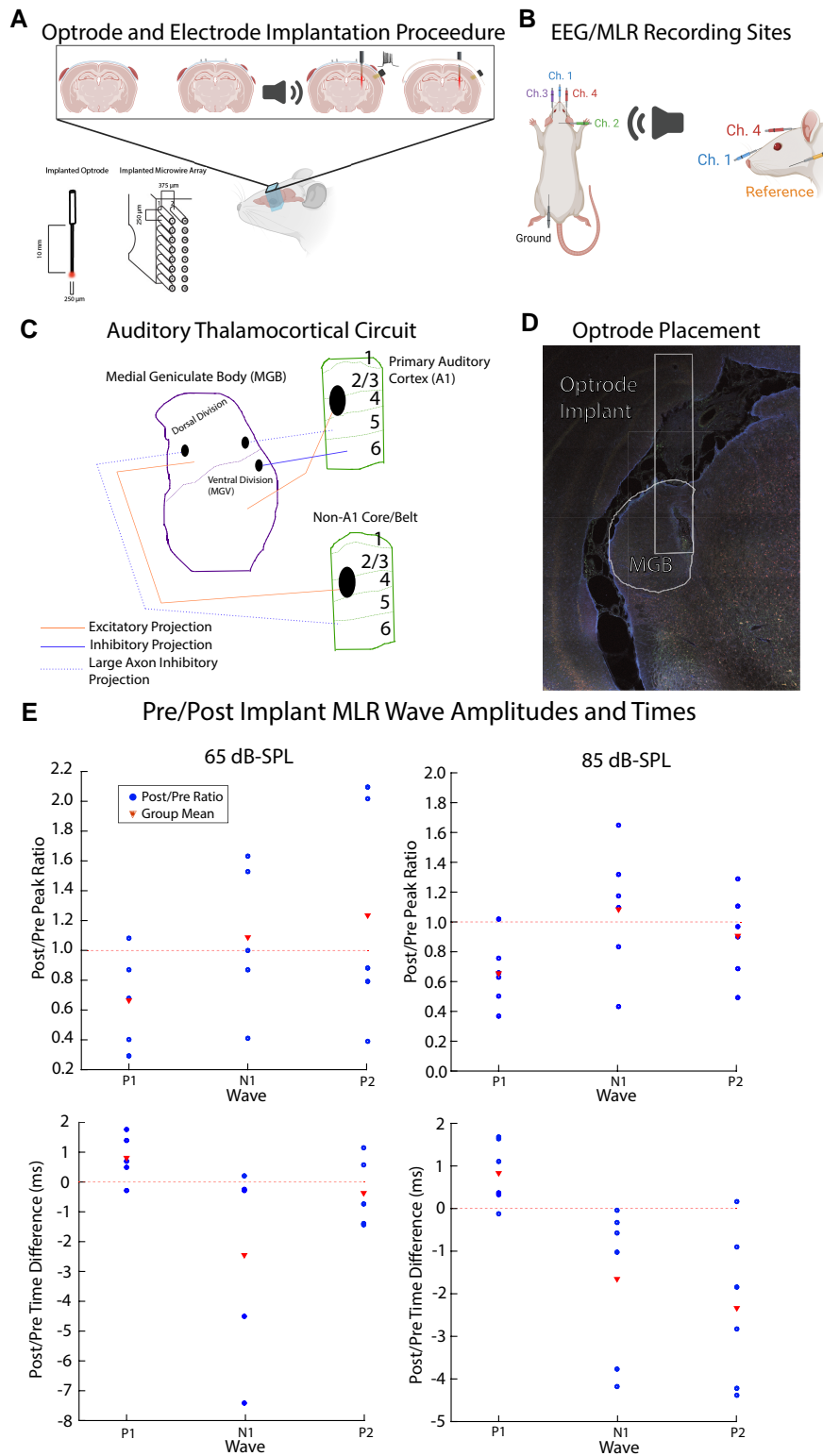


**Fig. 1.** Implantation and EEG-MLR procedures. A) Rodents were implanted with fiber optic optrodes into the MGB and 16 channel microwire arrays into auditory cortex. Placement of microwire array was confirmed by tonic single-unit responses evoked from 80 dB filtered Gaussian noise stimuli during implantation. B) Schematic of the four-channel EEG-MLR recording preparation. C) Schematic of the rodent auditory thalamocortical circuit. Stimulation optrodes were placed in the MGB with excitatory thalamocortical projections to layers 3–4 of primary and secondary auditory cortices. Microwire array recording electrodes were placed in layers 3–4 of primary auditory cortex confirmed during surgery by low-latency single-unit activity. D) Histological confirmation of stimulation optrode placement in the MGB. E) EEG-MLR prepostsurgical ratios show small changes in wave P1, N1, and P2 correlates of auditory thalamocortical function in amplitude and latency due to passive presence of device at 65 or 85 dB-SPL click stimuli. While changes in amplitudes and latencies were observed, differences did not rise to level of significance ( $P > 0.05$ ). Rodent implantation and EEG diagrams were created using BioRender ([www.biorender.com](http://www.biorender.com)) under publication license.

evoked MLR in a subset of rats ( $n=6$ ). MLR stimuli consisted of evoked responses to auditory click trains with recordings taking place 24 h before and 72 h after implantation procedures. MLRs report auditory generators in thalamus and cortex and serve as a read-out of neural ensemble function (62–65). We utilized a four-positive channel electroencephalography (EEG) recording configuration to allow for responses of thalamocortical generators and rostral brainstem regions (54) (Fig. 1A, right) on each hemisphere. We analyzed ratios of postpre positive peaks 1 and 2 (P1, P2) corresponding to brainstem and cortical generators, respectively, and negative peak 1 (N1 or N1-P2) corresponding to thalamic generators (Fig. 1B). While there was some variability in wave amplitudes and latencies, comparisons of evoked activity resulting from click-train auditory stimuli at 65 and 85 dB-sound pressure level (SPL) (Fig. 1E) showed no significant difference in response ( $P > 0.05$ , Wilcoxon sign-rank) suggesting that presence of stimulation optrodes and recording electrodes did not significantly damage or alter thalamic and cortical activity at the onset of INS experiments. Moreover, it allows for the possibility of residual hearing circuits working in concert with INS for optimal hearing function. It should be noted that postsurgical recordings were performed 72 h after surgery, well within the device heal-in window (66), with further neural reorganization likely to occur throughout the duration of the study.

### Dose-response relationships of cortical neuron response from thalamic INS

We next examined the interplay of INS laser energy and interstimulus pulse intervals (ISI) on evoked cortical single-unit firing rates. To estimate the firing rate and timing of INS-elicited single-unit activity, peristimulus time histograms (PSTHs) were constructed (67, 68) (Materials and methods: Data processing and analyses) with true instantaneous firing rate functions estimated using Bayesian adaptive regression splines (BARS) (69–71). PSTHs of single units which were responsive to INS stimuli (Z-score increase  $\geq 7.84$  from basal firing rate,  $P < 0.00001$ ) were analyzed. Units showing inhibitory responses or no change from basal firing rates were excluded from the present study. Examples of PSTHs and estimated instantaneous firing rate functions elicited from graded INS activation in A1 are shown in Fig. 2A. While INS dose-response relationships have been studied in cortex (23, 24), they remain unstudied across thalamocortical networks. Dose-response profiles were modeled as a Bayesian hierarchical linear random effects regression model, allowing us to account for hierarchical structure of data consisting of variability within and between subjects across implantation lifetimes. Bayesian inference is particularly powerful for this model as it provides complete quantification of posterior distributions over all regression parameters and allows for direct uncertainty quantification of parameters. Bayesian hierarchical regression models can be viewed as akin to frequentist mixed-effects models but offering improved estimation of groupwise variance (72, 73), improved estimation of effect size (74), and robust quantification in error uncertainty (75–77). Inference was performed directly on observed data posterior distributions. As Bayesian methods require specification of prior probability distributions for inference, broad, noninformative normal prior distributions were used in inference models. Prior sensitivity analyses were performed in order to ensure prior distributions did not unduly influence inference (Fig. S5 and Table S2). Dose-response regression models took the form of

$$\max(\text{FR}) = \alpha_i + \beta_{1,i} * E + \beta_{2,i} * \text{ISI} + \beta_{3,i} * (E * \text{ISI}) + \epsilon_i$$

with response variable FR representing the natural log-transformed evoked firing rate and independent variables  $E$  and ISI being the natural log transformed energy per pulse and interstimulus interval, respectively. The  $\beta$  terms are regression coefficients quantifying the effect of INS energy, ISI, and energy-ISI interactions on evoked firing rates from animal/electrode group  $i$ . The  $\alpha$  term corresponds to the regression intercept and is interpreted as the basal firing rate of animal/electrode group  $i$ . Model structure is shown in Fig. S1. Natural log transformations of response and independent variables were chosen as model terms after sensitivity analyses which dictated that log-transformed models best fit observed data (Fig. S5). An error term of  $\epsilon$  was added for uncertainty quantification. Full model descriptions and sensitivity analyses are provided in SI:Bayesian model description (Figs. S1–S9). Bayesian inference estimates the distribution of likely regression parameters from observed data (78). Regression parameters were summarized by their maximum a priori estimate (MAP) (i.e. most probable value) with independent variables considered significant contributors to response if the highest-density interval (HDI) of the parameter distribution corresponding to the 95% most probable parameter values did not overlap 0, following Bayesian inference convention (75). Significant regression parameter MAP estimates quantify change in evoked firing rates per unit change of laser energy and ISI, respectively. Uncertainty of regression parameter estimates is given in the spread of parameter distributions obtained from observed data. Regression models (Fig. 2B) show that INS responsive units had a basal firing rate  $>0$  ( $\alpha$  MAP = 2.2, 95% HDI excludes 0) with max evoked firing rates depending significantly on applied laser energy ( $\beta_1$ , MAP = 0.58, 95% HDI excludes 0) but not on ISI ( $\beta_2$ , MAP = -0.055) or energy-ISI interactions ( $\beta_3$ , MAP = 0.028). However, the relatively wide spread of the ISI parameter  $\beta_2$  across 0 suggests a potential critical point in ISI timing past which thalamocortical neurons are unable to entrain to individual pulses and instead integrate INS pulses into a single network event. Taken together, INS pulse energy is the primary driver of evoked neural firing rates, with increasing energy per pulse leading to increased maximum firing rates.

### Cortical encoding of INS stimuli

We next used Shannon mutual information measures [ $I(R; S_x)$ , Supplementary Methods 3.2] to assess and quantify information carried by evoked spike-trains in response to INS stimulation energy. Mutual information measures the reduction of uncertainty in neural response ( $R$ ) given knowledge of the particular stimulus ( $S_x$ ). Higher values of information represent more unique and separable encoding of neural response distributions for each stimulus. Stimulus-information profiles were calculated from 5 ms binned estimates of response probability mass distributions during INS conditioned on applied energy. Bias in mutual information resulting from incomplete knowledge of population response distributions was estimated and corrected using the methods of quadratic extrapolation (79, 80). We found that increasing INS energy per pulse resulted in increases in information contained in response spike trains (Fig. 2C). Increases in information are also positively correlated with increased INS energy per pulse showing strong dependence of evoked PSTHs on laser energy, particularly  $>0.8$  mJ/pulse (Fig. 2C).

Auditory thalamocortical circuits perform complex transformations of inputs at the auditory thalamocortical synapse (81) with cortical neurons employing differential coding strategies across local heterogeneous cells and circuits (82, 83). Therefore, it is imperative that any stimulation modality be able to drive

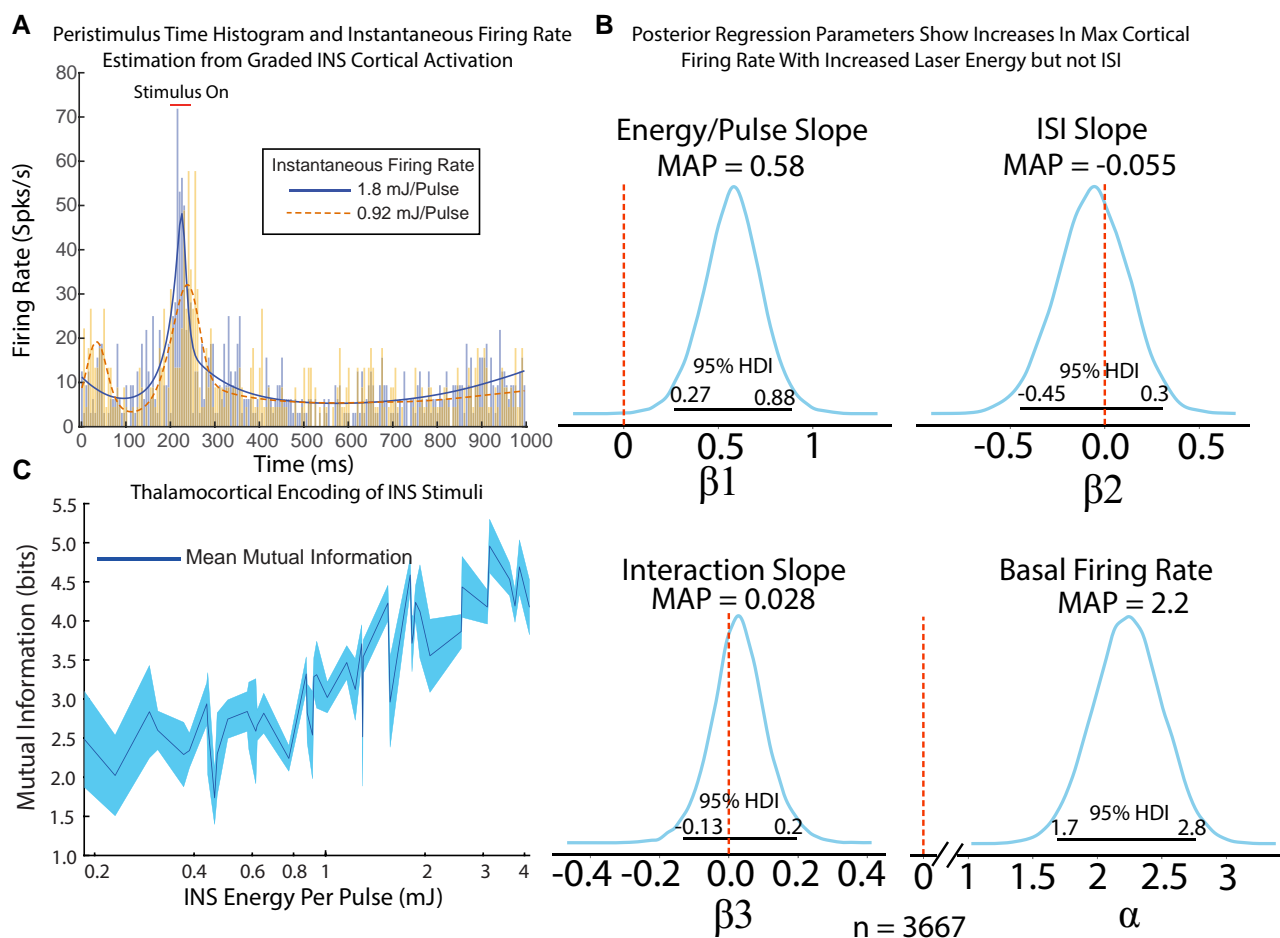


**Fig. 2.** A) Example INS-evoked PSTHs. BARS estimates of 1.8 mJ (solid line) and 0.92 mJ (dotted line) per pulse show higher energy pulses drive higher firing, lower latency responses. B) Bayesian hierarchical linear regression models of cortical dose-response profiles elicited by INS describe the effects of varying INS parameters on evoked firing rates. Distributions of regression parameters as estimated from observed data are given for applied laser energy (top left), laser interstimulus interval (top right), and laser energy-interstimulus interval (bottom left) interactions. Assessment of statistical significance was made using the Bayesian convention of HDI estimation. Distributions of regression parameters are shown, with parameters being significant if 95% of parameter value distribution does not contain null value 0 (vertical dotted line). Regressions show that increases in applied energy significantly increase maximum cortical firing rates with a maximum a priori estimate of 0.58 increase in log firing rate in response to increases in log energy (95% HDI does not overlap 0). The width of the 95% HDI of the energy parameter (0.27–0.88) suggests that while cortical firing rates increase with increases in laser energy generally, total increase in maximum firing rates per unit change in INS energy is dependent on the physiology of the neuron. Slight decreases in firing rate with increased ISIs were observed (MAP =  $-0.055$ ), but not significant (95% HDI overlaps 0). Laser energy and ISI interactions also did not significantly change evoked cortical firing rates (95% HDI overlaps 0). Basal firing rates (bottom right) of neurons were significantly above 0 (95% HDI does not overlap 0, MAP estimate = 2.2). C) Evoked single-unit spike train MI increases as INS energy increases (standard error presented as shaded error bars).

naturalistic response profiles. INS-evoked PSTHs were classified into onset, sustained, onset-sustained, and offset categories representative of the known range of possible responses (84) (Fig. 3A). PSTHs showing poststimulation drop of 95% of basal activity were assigned an “inhibitory” flag corresponding to presence of poststimulus inhibition. Classification results are summarized in Table 1. Onset responses were the most represented class (onset + inhibition: 49.93%, onset: 12.04%) followed by sustained (sustained: 18.78%, sustained + inhibition: 4.51%) and onset-sustained classes (onset-sustained: 6.05%, onset-sustained + inhibition: 2.82%). Offset responses were the least observed class (5.87%). Observed distributions of firing classes are supported by studies of auditory evoked cortical unit responses (84) showing similar distributions of onset, onset-sustained, sustained, and offset responses in cortical layers III/IV as observed in our data, suggesting that INS drives naturalistic thalamocortical encodings.

While these response states were categorically divided into possible response classes (84), these categories are not meant to

suggest all responses fit neatly into well-defined clusters. Principal components analysis (PCA) dimensionality reduction was performed on response profiles to assess the extent to which responses fall on a continuum. Dimensionality reduction into the top three components of largest variance (65.11% variance explained) shows that while responses do form some identifiable clusters, responses fall on a continuum of responses within a given cluster (Fig. 3B), suggesting INS does not only generate singular stereotypic responses but drives biophysically relevant responses across the thalamocortical synapse. Bayesian multinomial regression models (Supplementary Methods) were utilized to infer whether firing class membership was solely a function of INS stimulation parameters. Multinomial regression compares log odds of a PSTH belonging to a given category against a reference category. The most populous onset + inhibition category was chosen as reference. Models suggest that class membership is a function of INS energy and ISI, with movement from onset + inhibition to onset resulting from increases in energy and ISI,

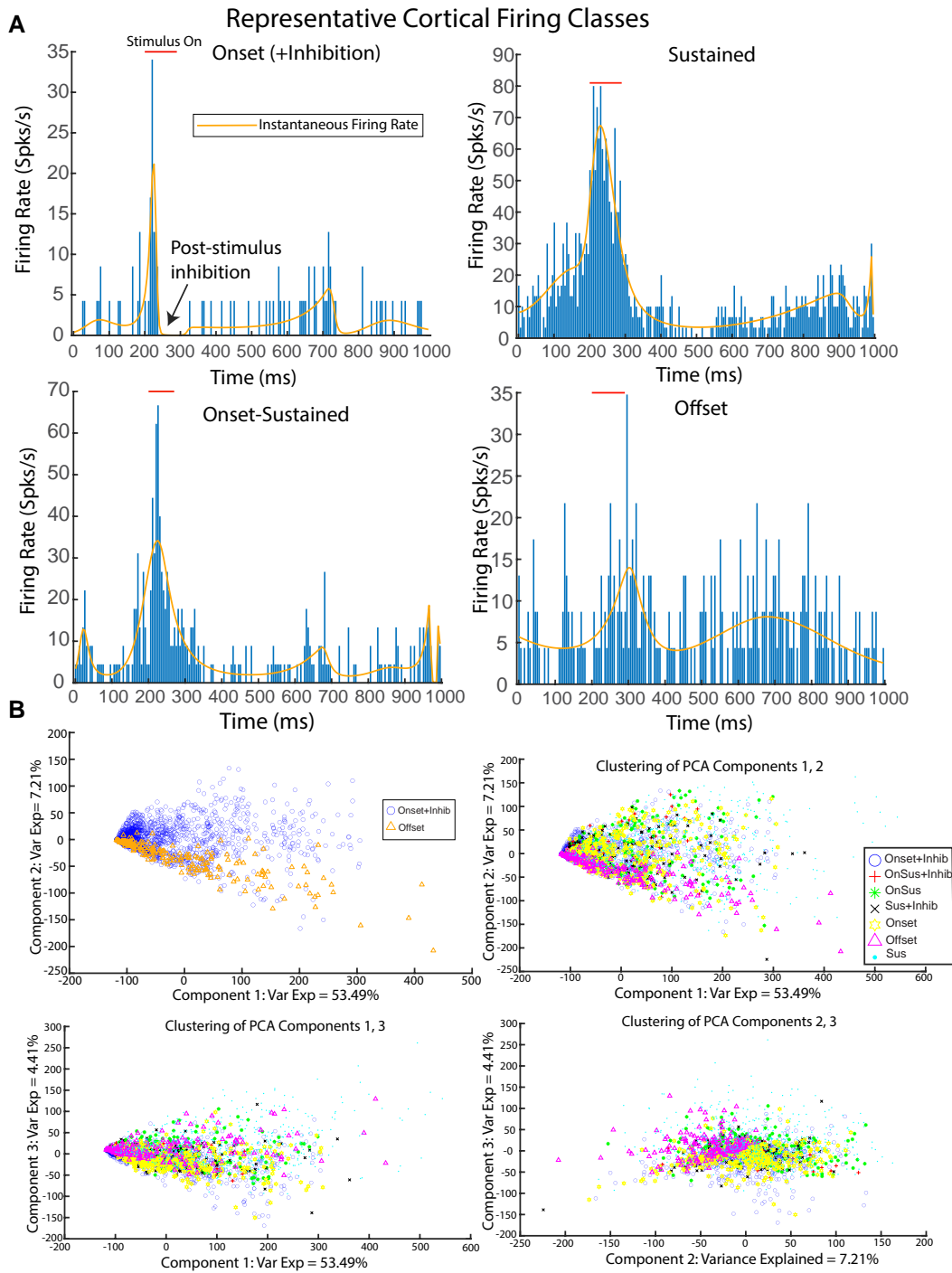


**Fig. 3.** Examples of auditory cortex firing classes evoked from INS stimuli. A) Evoked cortical firing activity was classified into onset, onset-sustained, sustained, and offset classes. Responses were classified as onset if INS induced a significant increase in firing activity above spontaneous activity compared to the 200 ms prestimulus window with a return to spontaneous firing rates before cessation of INS stimuli (top left). A response was classified as sustained if INS elicited a significant increase in firing rate above spontaneous rate that maintained firing rates of at least  $\frac{\text{onset rate}}{\text{sustained rate}} < 3$  through the duration of the stimulus (top right). Responses were classified as onset-sustained if INS elicited a significant increase above spontaneous rate with sustained activity above a firing rate of  $\frac{\text{onset rate}}{\text{sustained rate}} \geq 3$  (bottom left). A response was classified as offset if firing rates significantly increased from spontaneous rates after cessation of INS stimulus (bottom right). Onset, sustained, and onset-sustained responses received an additional classification of inhibition if poststimulus firing rates fell below 95% of mean prestimulus spontaneous rates. B) PCA decomposition was performed to assess if neural classes formed distinct clusters. Dimensionality reduction into the top three components of largest explained variance shows class specific clustering shapes with overlap between classes, suggesting that evoked responses are not uniquely stereotyped into fixed classes, but exist across a continuum. This is exemplified in (B), top left where PCA clustering of onset and offset classes into top two coefficients of explained variance show clusters with defined shapes and strong overlap of offset clusters into a subsection of the onset space. The decomposition of all classes into top three components of explained variance is shown in (B) top right, bottom left, and bottom right, respectively.

**Table 1.** Distribution of cortical firing classes ( $n = 3,371$ ).

Firing class	% of responses	% of responses in class
Onset	12.04	61.97
Onset + inhibition	49.93	
Sustained	18.78	23.29
Sustained + inhibition	4.51	
Onset-sustained	6.05	8.87
Onset-sustained + inhibition	2.82	
Offset	5.87	5.87

movement to onset-sustained resulting from decreases in energy and ISI, movement to onset-sustained + inhibition resulting from slight decreases in energy but large decreases in ISI, movement to sustained + inhibition resulting from larger decreases in ISI, and movement to offset class resulting from large decreases in applied energy and smaller decreases in ISI (Fig. S12). These models suggest an interplay between INS stimulation parameters, network dynamics, and intrinsic cellular biophysics determines response profile class.

### INS induces spatially constrained thalamocortical recruitment

We next investigated the spatial selectivity of thalamocortical INS using JPSTH analyses. JPSTHs allow for the assessment of the time-resolved correlation between pairs of neurons in response to both direct INS stimuli and poststimulation correlated activity (JPSTH formulation detailed in Fig. 4A). We utilized the spatial geometry of the implanted planar recording arrays to assess INS-induced correlated activity between pairs of neurons as a function of distance, with distance 0 corresponding to neurons recorded on the same channel. We first assessed stimulation-induced correlations of activity related directly to the stimulation event (Fig. 4A, left). We next calculated the JPSTH with direct stimulus effects removed, representing functional connectivity between compared neurons after secession of the stimulus (Fig. 4A, middle). The maximum correlated activity from all energies and distances was calculated to obtain an upper bound of lateral stimulation spread. Previous electrical mapping studies in rodent auditory thalamocortical areas using linear, Michigan-style arrays in nearly all cases showed electrical stimulation spread across the entire extent of recording arrays, up to 1,900  $\mu\text{m}$  (85, 86). INS correlation analysis shows all responses were constrained to  $\leq 1,500 \mu\text{m}$ , with 90% of responses constrained to  $\leq 1,000 \mu\text{m}$  (Fig. 4B, left). We next recalculated maximal spread for active units at stimulation intensities  $<1 \text{ mJ}$ , corresponding to an inflection point of increased stimulus transmitted information (Fig. 2C), to assess if maximum spatial spread is modulated by INS intensity. At lower energy stimulation, maximal spatial spread was limited to  $<1,250 \mu\text{m}$ , with 90% of responses constrained to  $\leq 750 \mu\text{m}$  (Fig. 4B, right), including numerous instances of moderate correlation  $\leq 500 \mu\text{m}$ . These data suggest maximal spreads of INS-induced activity is significantly less than electrical stimulation. Spread of activation after accounting for direct costimulation induced by INS shows similar results, with spreads of poststimulus correlated activity limited to 1,250  $\mu\text{m}$  across all energy levels and 1,000  $\mu\text{m}$  for energies  $<1 \text{ mJ}$  (Fig. 4C).

### Closed-loop control through deep reinforcement learning

After observation of spatial selectivity in thalamocortical INS, we sought to control small neural populations through closed-loop feedback. Current adaptive DBS systems used in Parkinson's

disease use relatively simple control algorithms centered around reducing  $\beta$  band biomarker correlates of symptomology using single or dual threshold “thermostatic” control (43, 87, 88) which may interfere with activities such as volitional movement (43) and may potentially occlude oscillatory neural dynamics unrelated to disease (40). Control of smaller populations of neurons relevant to disease with control algorithms that encode subject-specific firing dynamics may provide targeted treatment and a reduction in off-target side effects. We utilized deep RL to learn complex stimulus-response dynamics in real-time while finding stimuli to reach a desired firing state. State, in this study, refers to discrete classes of dynamical activity with stereotyped spontaneous and stimulus-evoked activity (89). RL consists of a computational agent that takes actions in response to observations of a given neural state and learns which actions to take to maximize current and future rewards. In our deep RL paradigm, termed SpikerNet, the RL agent can take actions from an action space consisting of INS stimulus parameters of laser energy, ISI, and number of pulses which are constrained to consensus safe energy levels. Stimuli are applied in response to observation of neuron PSTHs from recording electrodes. A reward was then calculated by quantifying mean-squared-error (MSE) distance between evoked firing and target PSTHs. Action policies and state response relationships are then learned using actor-critic deep neural networks, with the actor-network encoding actions to take in each environment and the critic learning present and future rewards of taking a given action (Figs. 5A and S13).

We have previously shown in computational models that SpikerNet is able to quickly learn stimulus trajectories to achieve desired firing patterns (40). SpikerNet's ability to achieve desired firing patterns in vivo was tested by sampling from distributions of previously evoked responses to create novel, previously unobserved firing response target states for the recorded unit. We determined SpikerNet was able to find target firing states precisely (Fig. 5B,  $\text{MSE} = 3.872$ ) within a limited number of search iterations (Fig. 5C) as predicted in our computational studies (40). It should be noted that search dynamics are intrinsically stochastic and unique to a given animal, target response, and algorithm seeding. Search trajectories during training stages show rapid discovery of target responses indicated by low mean square error followed by exploratory behavior away from the target (Fig. S13), characteristic of RL sampling of action-response distributions (90) and necessary to develop a full stimulus to response mapping. We also found that SpikerNet exploration generated a wide variety of firing classes during search that was not identified during our standard intensity and ISI stimulation protocol, including onset-inhibition responses (Fig. 5D, trials 0 and 2), sustained activity followed by burst offset response (Fig. 5D, trial 12), and multi-peaked sustained responses (Fig. 5D, trial 22). The ability to create and observe such diverse firing patterns is critical to learning stimuli to generate any firing state as well as relearn stimulus-neural dynamics as responses change due to age of recording and stimulation devices and neural adaptation over time.

## Discussion

In this study, we demonstrated INS as a viable oDBS method for treatment of circuitopathy-related neurological diseases and disorders. We quantified INS dose-response profiles and stimulus-response information transformations while also showing the ability of INS to drive biophysically relevant cortical responses at safe energy levels. We further show that INS provides spatially specific activation in thalamocortical networks with spread well below conventional electrical stimulation. Finally, we leverage the

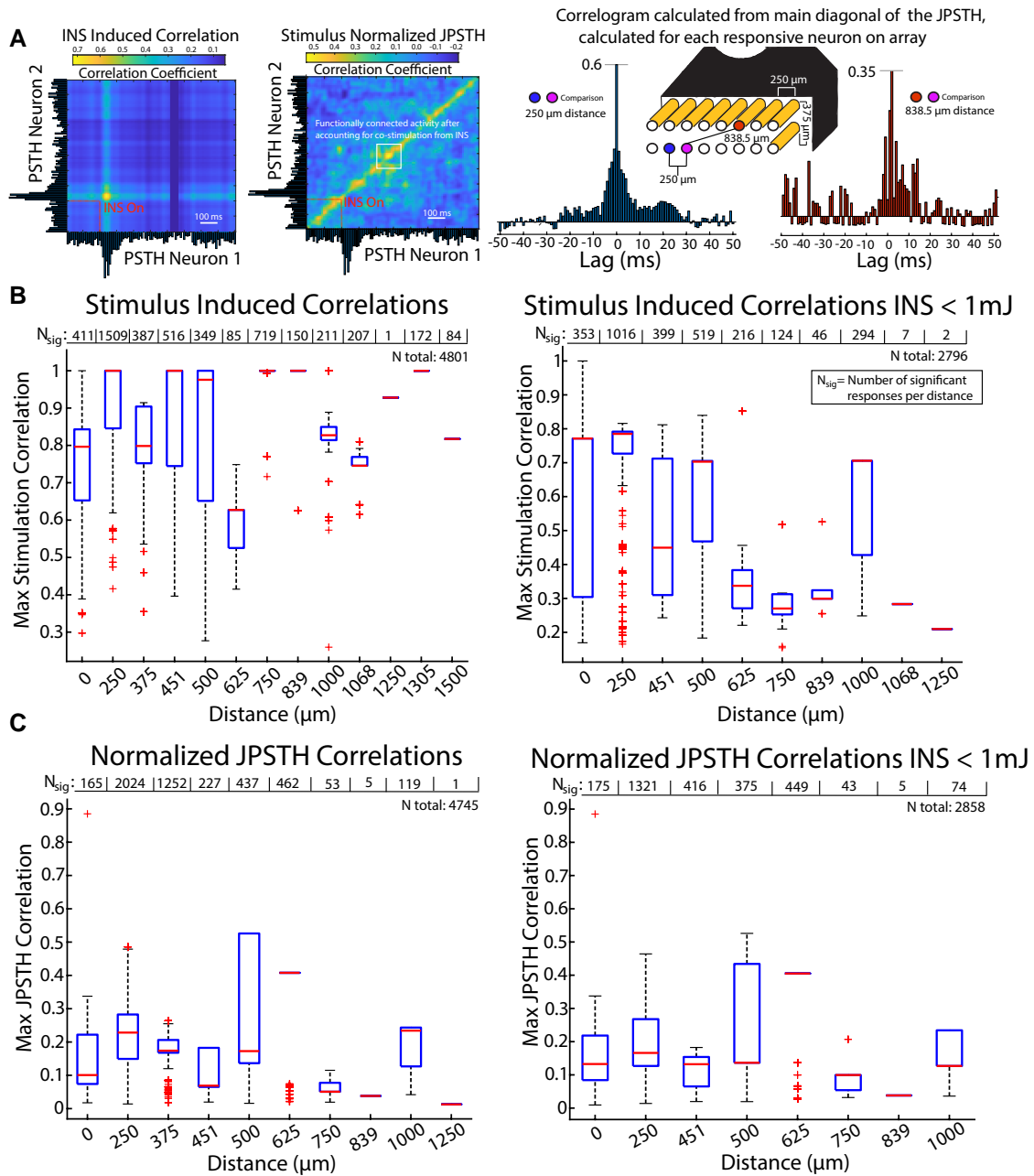


**Fig. 4.** JPSTH analysis reveals INS thalamocortical recruitment is spatially constrained. A) JPSTH methods quantify the correlation dynamics of pairs of neurons. For each INS condition, PSTHs for two neurons are time-aligned on an orthogonal axis. A JPSTH matrix is created by counting coincidences of spikes for both PSTHs across all time normalized to the variances of both PSTHs, creating a time-varying covariance response to INS stimuli, where events occurring across the lower left to upper right (the main diagonal) correspond to correlations close in time. Then, the stimulus normalized JPSTH matrix is calculated by creating a JPSTH with one neuron shifted in time by one stimulus trial, which is subtracted bin-by-bin from the original JPSTH to remove physiologically induced correlations arising after the primary INS stimulation train. The normalized JPSTH represents long-term correlated functional connectivity after accounting for direct INS-induced responses. JPSTHs were calculated for all INS responsive neurons on the recording array. Cross-correlograms were calculated by summing coincident firing in diagonal bins oriented in the direction of the main diagonal of the JPSTH, normalized by bin length. JPSTH matrices were smoothed by a two-dimensional Gaussian smoothing kernel with variance of three for visualization. All reported correlations and JPSTHs were calculated from raw, unsmoothed covariance histograms. Statistical significance of correlations was assessed via shuffled permutation testing. B) Bar plots of maximum correlations vs. distance. Distances of 0 correspond to neurons recorded on the same electrode. INS-induced response correlations (left) show that spread of activation within cortical layers III/IV was constrained to a lateral spread of  $\leq 1,500 \mu\text{m}$  with 90% of responses constrained to  $\leq 1,000 \mu\text{m}$ . Laser energies  $< 1 \text{ mJ}$  per pulse (right) further limited correlated lateral spread to  $\leq 1,250 \mu\text{m}$  with 90% of responses  $\leq 750 \mu\text{m}$ . C) Pairwise normalized JPSTH correlations (left) measuring poststimulation induced connectivity show layers III/IV cortical lateral spreads limited to  $\leq 1,250 \mu\text{m}$  with 90% of responses constrained to  $\leq 625 \mu\text{m}$ . Laser energies  $\leq 1 \text{ mJ}$  per pulse (right) further show poststimulation induced connectivity limited to  $\leq 1,000 \mu\text{m}$  with 90% of responses constrained to  $\leq 625 \mu\text{m}$ .



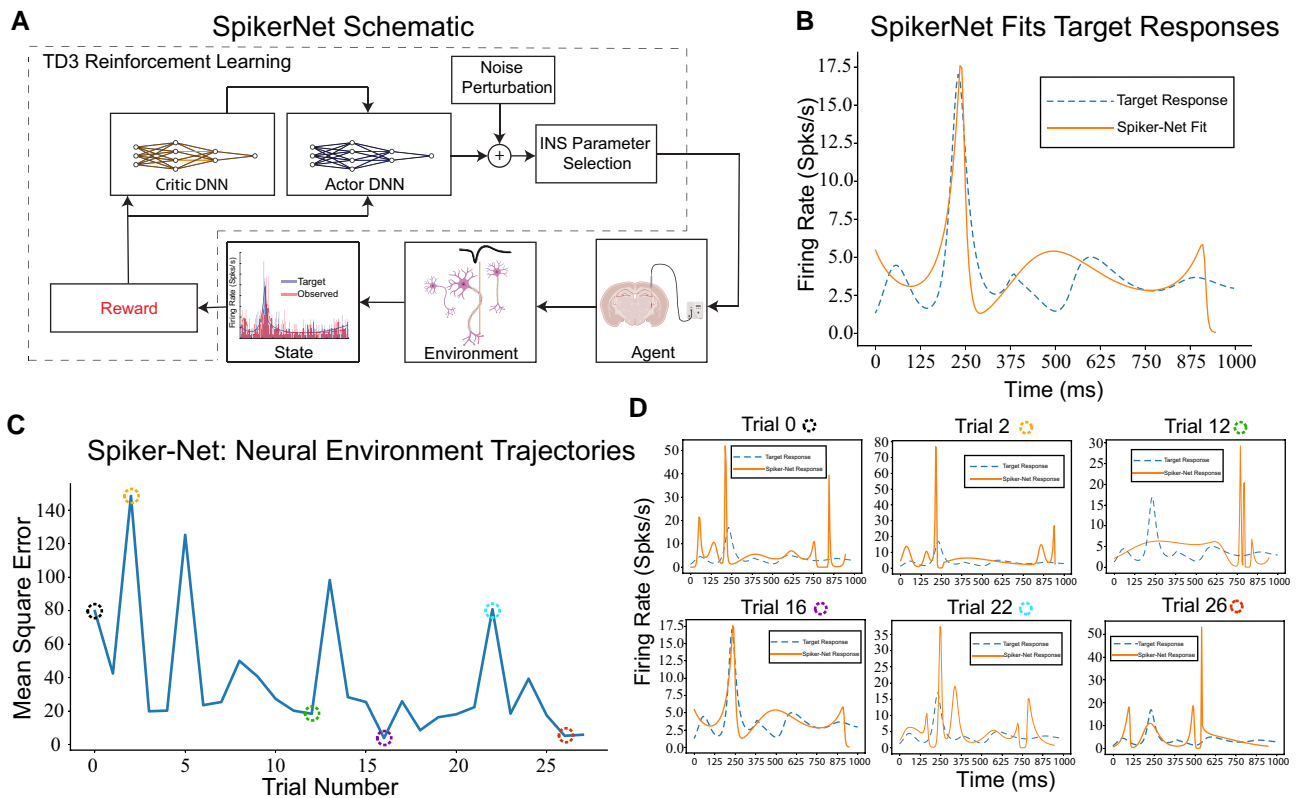


**Fig. 5.** SpikerNet, a deep RL-based closed-loop control system. A) Schematic of SpikerNet operation, which utilizes TD3 RL. The state is representative of a response as recorded from the electrode environment. The agent is the set of all safe stimulation parameters. B) SpikerNet is able to find arbitrary neural firing patterns through repeated iterations of stimulation through the environment. C) SpikerNet partakes in search and targeting behavior to find target responses and to learn stimulation parameters that best drive the neural environment to target state. D) Example evoked responses during SpikerNet search and learning show a wide variety of firing classes are evoked during algorithm search. While fits were calculated around the window of evoked activity (200–300 ms), more complex multi-peaked and offset responses were observed (trials 12, 22, and 26).

spatial specificity of INS to derive a deep RL-based closed-loop optical control system that can drive neural responses to target states.

### INS drives physiological thalamocortical responses

While many previous INS studies have explored the role of wavelength dependence on INS activation (22, 91, 92), dose-response relationships have largely not been studied. Activation profiles are critical for therapeutic dosing of neuromodulation therapies to titrate efficacious pulses while minimizing patient discomfort from overdriving neurons. Dose-response curves show exponential increases in maximum firing rates in response to increased laser energy with some evidence that extremes in ISI further shape neural response PSTHs through integration of INS pulses close in time (Fig. 2A and B). One caveat to our study is that only excitatory responses were considered. It has been observed that continuous pulse-width or high frequency ( $\geq 200$  Hz) INS stimulation can drive selective inhibitory responses in nerve through introduction of a thermal block (93–95), though this type of stimulation can produce longer-lasting mixed excitatory and inhibitory responses, with a higher proportion of excitatory responses for lower stimulus energies (96). The MGB sends excitatory glutamatergic projections to A1, and a small proportion of collaterals synapse onto GABAergic parvalbumin-positive interneurons (97) which facilitates feedforward inhibition in cortical cells. We observed some evidence of inhibitory responses, showing decreases in basal firing rate following INS stimulation. These responses were excluded

from further analysis in the study given their scarcity with the INS parameters tested. However, controlled induction of inhibitory responses should be studied as a means to enhance and diversify A1 neural coding strategies in future studies using higher-density recording arrays and stimulation optrodes. An understanding of joint excitatory and inhibitory effects of circuitual INS would potentially allow for bidirectional control of local microcircuits and is planned for further study.

INS of thalamocortical neurons produced a variety of short-latency peristimulus responses in auditory cortex neurons, comparable to sound-driven auditory cortex responses across species (84, 98–101). These results suggest that thalamocortical INS stimulation largely preserves natural network activation, as evidenced by preserved A1 response class distributions between INS and auditory stimulation and including sustained responses where the response outlasts the stimulus as well as inhibitory responses. Conservation of response classes between auditory stimulation and artificial INS suggests they drive comparable thalamic firing patterns. Our INS stimulation parameters differed from previous INS studies in somatosensory cortex with our responses more closely resembling MGB firing rates (52, 102). There is evidence that DBS imparts its therapeutic effect partially through activation of motor cortex from antidromic activation of subthalamic nucleus collaterals (103). While our study can't strictly rule in or out similar antidromic activation of thalamocortical targets, given that ventral MGB largely sends afferent projections to layer III/IV of A1, INS activation in the present study is likely driven by orthodromic stimulation.

## Spatial selectivity of thalamocortical INS

A oft-touted advantage of INS for cochlear/peripheral (17, 26, 32) and cortical neuron (24) stimulation is constrained stimulation. However, there historically has been a dearth of understanding of network responses and spread of activation through synapses elicited from INS. Previous studies have often focused on intrinsic optical and calcium imaging recordings of cortical cells from direct INS stimulation (23, 24, 104). Here we show that INS drives spiking responses across the thalamocortical synapse within a constrained region that is significantly smaller than the region affected by equivalent electrical stimulation. At low INS stimulation energies, activation could be  $\leq 500 \mu\text{m}$ , and even at saturating energy levels for firing rates, activation was typically less than  $1, 500 \mu\text{m}$ . It is possible that the activation spread at low energies could be even more restricted, given that we were not able to measure spread of activation in the immediate vicinity of the implanted optrode and that we did not optimize thalamus/cortex overlap in our implantation. Both anatomically and electrophysiologically in A1, there are matched reciprocal projections between the auditory thalamus and cortex (105, 106). Additional mapping during implantation surgery to identify most effective stimulation sites for a given cortical site may reduce energies needed or increase informational capacity even further. As hybrid recording electrodes fixed with optrodes are in use in optogenetic studies, it is feasible to fabricate similar recording arrays with optics that pass near-infrared stimuli, allowing for the study of joint activation and spread in thalamus and cortex concurrently. Regardless, our results show finely graded thalamocortical recruitment, which would potentially reduce off-target stimulation side-effect profiles in oDBS applications. Further constrained stimulation could also be set during the programming stage of an oDBS system, potentially allowing for fine tuning of therapeutic stimulation.

## Clinical viability of INS

This study lays the significant groundwork for the preclinical development of INS for use in a spatially constrained oDBS system. Furthermore, INS has already shown promise in human nerve mapping (32) and intracortical microstimulation (107). However, significant hurdles remain for translation of INS. Laser parameters necessary for stimulation have high optical energy (1–4 mJ) requirements, making fully implantable devices technically challenging. Much progress is currently being made in implantable infrared systems that satisfy requirements for stimulation which could be realizable on implantable pulse generators (IPG) (108). Safety profiles of INS are also promising, with tissue ablation thresholds well studied (30–32, 109, 110). While our data suggests INS drives biophysically relevant responses across a diversity of cell response patterns, disease models are necessary to fully assess therapeutic potential of INS as a DBS paradigm. The biophysical mechanisms of INS are still in debate, with transient thermal gradients (111, 112), transient cellular capacitance changes (113, 114), intracellular calcium cycling (115, 116), intrinsic ion channel light transduction (28, 117), or combinations thereof suggested as causative mechanisms of INS. While not directly assessed within this study, observed short-latency, fast-spiking responses suggest primary ion channel mediation of INS as opposed to slower intracellular calcium signaling. In vitro whole cell and outside-out patch-clamp studies could elucidate the interplay of the intracellular and membrane-bound ion channel sequelae of transient and local thermodynamic changes. A better understanding of these photon-neuron interactions could give rise to more efficient

stimulation with larger margins of safety for use in clinical settings.

## Closed-loop reinforcement learning-based DBS

Closed-loop DBS provides key advantages over conventional open-loop DBS, including improved stimulation efficacy, reductions in side effects, and longer IPG battery life (42, 118). However, current closed-loop approaches are limited by non-specific activation of neural targets (88) and relatively simple, threshold-based control algorithms that have difficulty in deciphering pathologic and nonpathologic neural activity (40, 43). We developed SpikerNet to take advantage of spatial selectivity found in INS while also allowing for robust learning of complex neural firing patterns in real-time. An advantage of RL over other deep neural network paradigms is that statistical models of neural firing patterns are learned in situ and are specific to a subject's unique neural responses, requiring little training time and not requiring retraining or recalibration. We show that SpikerNet rapidly finds and fits targeted firing patterns (Fig. 5B) with search behavior that suggests the ability to fit a wide range of possible neural firing patterns (Fig. 5C). We have previously shown in computational models that SpikerNet is flexible to drastic changes in firing patterns (40) suggesting that SpikerNet can adapt to long-term changes in neural environments present in chronic, clinical DBS and can reduce the number of trips to the clinic for stimulator adjustments. We also observed evidence of SpikerNet finding target responses through the duration of a subject's recording period, during which arousal can significantly change firing responses requiring retuning of stimulus parameters (Fig. S13). Taken together, SpikerNet could serve as a powerful closed-loop DBS paradigm that can learn and adapt to changes in individual neural responses.

Deep neural network-based approaches, however, present a significant challenge for translation, in that algorithm decisions are typically made through a “black box” and ultimately unobservable system that may limit guarantees on device efficacy. RL methods however are advantageous in that the stimulus-response relationships after training can be directly observed in implanted devices, allowing for better inference on device operation. However, as stimulation policies are learned using deep neural networks, the salient neural state features leading to stimulus policy formation are still subject to the blackbox problem. The use of novel small network RL policy interpretability tools (119) with a posteriori evaluation of trained input/output responses can allow for a deeper understanding of algorithmic decision making. In this way, we see SpikerNet as a tool that can be utilized as a “physician in the loop” system, where SpikerNet can be utilized in concert with a trained DBS technologist to assist in difficulties found in DBS programming (120) and with physician monitoring during autonomous learning and stimulation.

## Materials and methods

All experimental and surgical procedures and protocols were approved by the Institutional Animal Care and Use Committee (PACUC) of Purdue University (West Lafayette, IN, #120400631) and in accordance with the guidelines of the American Association for Laboratory Animal Science (AALAS) and the National Institutes of Health guidelines for animal research. A total of 11 rats were used in this study. All animals received presurgical EEG-MLR recordings to ensure function of the auditory thalamocortical circuit. An initial subset of animals ( $n=6$ )

received postsurgical MLRs to assess the passive effect of device presence in the thalamocortical circuit. Inclusion criteria for chronic INS recordings included animals with functional optrodes and recording electrodes throughout the duration of the study. A total of seven animals met chronic recording criteria and were included in analysis.

## Surgical procedures

Adult Sprague–Dawley rats with weights between 300 and 400 g (Envigo, Indianapolis IN) were initially anesthetized in an induction chamber with 5% isoflurane and given a bolus injection of a ketamine/dexmedetomidine cocktail ( $70 \frac{\text{mg}}{\text{kg}}$  and  $0.2 \frac{\text{mg}}{\text{kg}}$ , respectively). Surgical plane of anesthesia was monitored continuously throughout the procedure by evaluation of toe-pinch reflex. A pre-operative analgesic dose of Buprenorphine ( $1 \text{ mg/kg}$ ) was administered 30 min before first incision and every 6–12 h for 72 h postsurgery. Rats were placed in a stereotaxic frame secured by hollow ear bars. An initial incision was made down midline with blunt dissection of periosteum performed to reveal cranial sutures. Three stainless steel bone screws were placed in the skull to ensure stability of implanted devices and headcap with a fourth titanium bone screw placed to serve as a ground and reference electrode (121). Right hemisphere temporalis muscle was gently resected and a  $2 \times 2 \text{ mm}$  craniectomy was made above auditory cortex (A1) (centered:  $-6$  anterior-posterior (AP),  $-5$  medial-lateral (ML)) (122). Dura was gently resected using a 25G curved needle. A  $2 \text{ mm} \times 2 \text{ mm}$  16 channel microwire array (TDT, Alachua, FL, USA, electrode spacing given in Fig. 1A) was inserted perpendicular to the surface of the brain. Devices were slowly inserted into A1 during application of 80 dB Gaussian noise stimuli. Devices were placed centered putatively in layer III/IV of A1 after confirmation of low latency, high amplitude multiunit activity was observed on the array (50, 123). One animal received a 3 mm linear array (NeuroNexus A1-16,  $200 \mu\text{m}$  between contacts) with contacts placed in A1 layers 3/4 in place of TDT planar array. A second craniectomy was made above the MGB ( $-6$  AP and  $-3.5$  ML) (50) and a fiber optrode (Thor Labs, Newton, NJ, USA) was placed  $-6 \text{ mm}$  into tissue (Fig. 1A). Recording arrays and fiber optics were sealed into place by application of ultraviolet-curable composite (Pentron, Wallingford, CT, USA). Rats were returned to their home cage and allowed to recover for 72 h before beginning of the recording regime.

## Electrophysiological recordings

All recordings were performed in a  $9' \times 9'$  electrically and acoustically isolated chamber (Industrial Acoustics Corporation, Naperville, IL, USA) with laser electronics placed outside of the chamber to prevent field interactions from high current pulses (124, 125). Before recording sessions, rats were given a bolus intramuscular injection of dexmedetomidine ( $0.2 \text{ mg/kg}$ ) for sedation (50, 54, 126). Optical stimuli were delivered via a custom made, open-source INSight system (all plans available at our Github repository: <https://github.com/bscoventry/INSight> and included in Supplementary Material) with a  $1,907 \text{ nm}$  semiconductor laser (Akela Trio, Jamesburg, NJ, USA) fiber coupled to the optrode with a  $200 \mu\text{m}$ , 0.22 numerical aperture fiber (Thor Labs FG200LCC). Laser stimuli were controlled via a RX-7 stimulator (TDT) and consisted of train stimuli with pulse widths between 0.2 and 10 ms, ISI between 0.2 and 100 ms, and energy per pulse between 0 and 4 mJ, below reported thresholds of laser ablation (29, 32).

Each recording trial was composed of a 200 ms prestimulus interval to facilitate spontaneous rate calculations, application of the train stimuli, and a poststimulus interval with total trial length equal to 1 s. Applied laser energies were randomized to limit effects from neural adaptation with 30–60 repetitions per pulse width/interstimulus interval combinations. Signals from recording electrodes were amplified via a Medusa 32 channel preamplifier and discretized and sampled at 24.414 kHz with a RZ-2 biosignal processor and visualized using Open-Ex software (TDT). Action potentials were extracted from raw waveforms via real-time digital band-pass filtering with cutoff frequencies of 300–5,000 Hz, with local field potentials extracted from real-time digital filters with bands 3–500 Hz. Chronic recordings were made through the lifetime of implanted optrodes and electrodes. To assess the impact of unilaterally implanted devices, pre, and postsurgery MLR EEG was performed. The experimental setup used has been described in detail in previous studies (55, 56) and further explained in Supplementary Methods.

## Data processing and analyses

Action potentials and MLRs were exported and processed using custom-written programs in the Matlab programming environment (Mathworks, Natick, MA, USA). Spikes were sorted into single units using superparamagnetic clustering methods in Wave-Clus (127). PSTHs were constructed by first aligning spike times to INS stimulation. The recording window (200 ms prestimulus and 1,000 ms total recording window) was divided into 5 ms nonoverlapping bins. The total number of spikes per bin ( $S_{\text{bin}}$ ) was counted with histogram bar height given by

$$H_{\text{bin}} = \frac{S_{\text{bin}}}{n\tau}$$

where  $n$  is the total number of trials for a given stimulus per recording session and  $\tau$  the total bin size of 5 ms. The resulting histogram has bin height  $H_{\text{bin}}$  in units of  $\frac{\text{spikes}}{\text{s}}$ . As PSTHs represent a noisy estimator of true firing rates, density estimation of true underlying instantaneous firing rate functions was calculated using BARS under a Poisson prior with  $\lambda = 6$  (69, 70). Calculation of instantaneous firing rate functions has been shown to better estimate true neural firing rates than raw PSTH estimates (71). Furthermore, BARS serves as a better estimator than conventional PSTH smoothing or frequentist approaches (70, 71).

Trials containing artifacts due to breathing or volitional movement were detected via between-channel cross correlation and RMS voltages exceeding 1 mV were removed from recordings. To facilitate comparisons between electrodes and animals, PSTHs were standardized using the following equation:

$$Z = \frac{\text{PSTH} - \mu_{\text{PSTH}}}{\sigma_{\text{PSTH}}^2}$$

where  $Z$  is the standardized PSTH and  $\mu$ ,  $\sigma_{\text{PSTH}}^2$  are the mean and standard deviation of the PSTH. Neurons were classified as responsive to INS if a PSTH in the stimulus series showed a z-score firing increase of  $\geq 7.84$  ( $4 * 1.96$ ,  $1.96 = \text{critical } Z\text{-score threshold}$ ) above mean spontaneous firing rate.

After detection and PSTH calculation, single-unit responses were sorted into one of seven established firing pattern classes found in rat auditory cortex (84, 128). Responses were first classified into onset, offset, sustained, or onset-sustained classes, with onset responses exhibiting a rise above spontaneous activity followed by a drop to spontaneous rates before cessation of the stimulation and offset responses characterized by an increase in

firing rate from baseline after termination of stimulus plus 7 ms to account for maximal response latencies in cortex from thalamic stimulation (128, 129). Responses showing firing activity above spontaneous activity throughout the duration of the stimulus were classified as sustained or onset-sustained, with onset-sustained responses showing a ratio of peak onset response to sustained rates  $>3$ . The inhibited response subclass showed a peri or poststimulus reduction in basal firing rate to below 95% of mean rate during the 200 ms prestimulus interval.

Mutual information (MI) measures of thalamocortical encoding of INS stimulation were calculated using the methods of Borst and Theunissen (114) with bias correction performed using quadratic extrapolation (63). Full information theoretic calculations are provided in the [Supplementary Methods](#). Lateral spreads of activation across cortical neurons were assessed through JPSTH analyses (130). Full JPSTH models and algorithmic descriptions are given in the [Supplementary Methods](#).

### Deep reinforcement learning-based closed-loop control

Closed-loop DBS control was achieved through a novel deep RL-based paradigm which we termed as SpikerNet (39). SpikerNet was programed in Python using the Pytorch deep learning backend (131). A custom made OpenAI Gym environment served as the interface between TDT data acquisition hardware and Pytorch. Deep RL seeks to maximize a target reward by continually sampling an environment while learning which actions taken provide highest future rewards through time (132, 133). In SpikerNet, the environment space was defined as the continuum of evoked cortical neuron firing rate PSTH densities. The action space was the continuum of stimulation amplitudes, pulse widths, and number of INS pulses delivered in a trial. The action space of stimulation parameters was limited in both hardware and software to below ablation thresholds to ensure SpikerNet did not damage thalamic structures during parameter search. Deep RL was performed using the twin-delayed deep deterministic policy gradients (TD3) algorithm, which is a model-agnostic double Q learning method for continuous environment and action spaces that outperforms other model-free deep-Q learning methods (134). To assess the ability of SpikerNet to reach arbitrary spike PSTHs, distributions of all observed PSTHs were formed. From that distribution, a target PSTH was sampled and represented a nonobserved but biophysically plausible target PSTH. Reward functions were set as

$$\frac{1}{\text{MSE}(\text{PSTH}_{\text{target}}, \text{PSTH}_{\text{observed}})}$$

with MSE chosen as it provides asymptotically the maximum likelihood estimator. Online multiunit PSTHs were calculated online from 10 repetitions of INS stimuli with densities estimated using online BARS. A MSE value  $<0.14$  denoted an observed result that is sufficiently close to the target response and acts as a signal to initialize a search episode. It is important to note that SpikerNet performs reward maximization through all episodes and is not truncated at the threshold of a sufficiently close fit.

### Statistical methods

All statistical methods, models, and sensitivity analyses are given in [Supplementary Methods](#).

### Acknowledgments

The authors would like to thank Dan Pederson, PhD and Kirk Foster for guidance in PCB layout and Don Ready, PhD for training,

maintenance, and funding of the Life Science Fluorescence Imaging Facility. The authors also thank the anonymous reviewers for their insightful and constructive feedback. B. S. Coventry is now affiliated with the Department of Neurological Surgery and the Wisconsin Institute for Translational Neuroengineering, University of Wisconsin-Madison, Madison, WI USA.

### Supplementary Material

[Supplementary material](#) is available at PNAS Nexus online.

### Funding

This study was supported by grants from the National Institutes of Health (NIDCD R01DC011580, PI: E.L.B.) and the Purdue Institute for Integrative Neuroscience collaborative training grant (PI: B.S.C.).

### Author Contributions

B.S.C. and E.L.B. conceived the study and acquired funding. B.S.C. and C.B.B. acquired EEG-MLR data. B.S.C. designed and built the INSight system, designed and programed SpikerNet, acquired single-unit responses, analyzed single-unit data, and performed immunohistochemistry and imaging. E.L.B. analyzed MLR data. G.L.L. conceived and wrote code for JPSTH analyses. B.S.C. and C.M.K. performed and assisted in surgical procedures. E.L.B. supervised the study. B.S.C. and E.L.B. wrote the manuscript. B.S.C., G.L.L., C.B.B., C.M.K., and E.L.B. reviewed and edited the manuscript.

### Preprints

This manuscript was posted on the bioRxiv preprint server at the following address: <https://doi.org/10.1101/2023.10.04.560859>

### Data Availability

All neural analysis and statistical inference code is available from <https://github.com/bscoventry/OpticalTCNeuromodulation>. Data used in this study can be found in the following open science framework repository: <https://osf.io/w4ufh/>. INSight INS system build files and materials list is available from: <https://github.com/bscoventry/INSight>. Due to patent restrictions, data and source code related to SpikerNet is available upon reasonable request from corresponding authors.

### References

- Harmsen IE, et al. 2020. Clinical trials for deep brain stimulation: current state of affairs. *Brain Stimul.* 13:378–385.
- Halbach M, et al. 2018. Baroreflex activation therapy for the treatment of heart failure with reduced ejection fraction in patients with and without coronary artery disease. *Int J Cardiol.* 266:187–192.
- Wu Y, et al. 2021. Deep brain stimulation in treatment-resistant depression: a systematic review and meta-analysis on efficacy and safety. *Front Neurosci.* 15:655412.
- Wu H, et al. 2000. Nucleus 21-channel auditory brainstem implant in patients with previous tumour removal. *Audiology.* 39: 247–252.

- 5 Medina M, et al. 2014. Cochlear implantation versus auditory brainstem implantation in bilateral total deafness after head trauma. *Otol Neurotol*. 35:260–270.
- 6 Gold JI, Shadlen MN. 2000. Representation of a perceptual decision in developing oculomotor commands. *Nature*. 404:390–394.
- 7 Salzman CD, Newsome WT. 1994. Neural mechanisms for forming a perceptual decision. *Science*. 264:231–237.
- 8 Dadarlat MC, O’Doherty JE, Sabes PN. 2015. A learning-based approach to artificial sensory feedback leads to optimal integration. *Nat Neurosci*. 18:138–144.
- 9 Dadarlat MC, Sun YJ, Stryker MP. 2023. Activity-dependent recruitment of inhibition and excitation in the awake mammalian cortex during electrical stimulation. *Neuron*.
- 10 Fisher R, et al. 2010. Electrical stimulation of the anterior nucleus of thalamus for treatment of refractory epilepsy. *Epilepsia*. 51:899–908.
- 11 Goodman WK, et al. 2010. Deep brain stimulation for intractable obsessive compulsive disorder: pilot study using a blinded, staggered-onset design. *Biol Psychiatry*. 67:535–542.
- 12 Tzadok M, et al. 2022. Rapid titration of VNS therapy reduces time-to-response in epilepsy. *Epilepsy Behav*. 134:108861.
- 13 Lujan JL, Crago PE. 2009. Automated optimal coordination of multiple-DOF neuromuscular actions in feedforward neuroprostheses. *IEEE Trans Biomed Eng*. 56:179–187.
- 14 Stickney GS, et al. 2006. Effects of electrode design and configuration on channel interactions. *Hear Res*. 211:33–45.
- 15 Noor MS, Murari K, McCracken CB, Kiss ZH. 2016. Spatiotemporal dynamics of cortical perfusion in response to thalamic deep brain stimulation. *Neuroimage*. 126:131–139.
- 16 Hemm S, et al. 2005. Deep brain stimulation in movement disorders: stereotactic coregistration of two-dimensional electrical field modeling and magnetic resonance imaging. *J Neurosurg*. 103:949–955.
- 17 Izzo AD, et al. 2007. Selectivity of neural stimulation in the auditory system: a comparison of optic and electric stimuli. *J Biomed Opt*. 12:021008.
- 18 Maks CB, Butson CR, Walter BL, Vitek JL, McIntyre CC. 2009. Deep brain stimulation activation volumes and their association with neurophysiological mapping and therapeutic outcomes. *J Neurol Neurosurg Psychiatry*. 80:659–666.
- 19 Cohen LT, Richardson LM, Saunders E, Cowan RSC. 2003. Spatial spread of neural excitation in cochlear implant recipients: comparison of improved ECAP method and psychophysical forward masking. *Hear Res*. 179:72–87.
- 20 Colletti V, Shannon RV. 2005. Open set speech perception with auditory brainstem implant? *Laryngoscope*. 115:1974–1978.
- 21 Wells J, Kao C, Jansen ED, Konrad P, Mahadevan-Jansen A. 2005. Application of infrared light for in vivo neural stimulation. *J Biomed Opt*. 10:064003.
- 22 Coventry BS, Sick JT, Talavage TM, Stantz KM, Bartlett EL. 2020. Short-wave infrared neural stimulation drives graded sciatic nerve activation across a continuum of wavelengths. *Annu Int Conf IEEE Eng Med Biol Soc*. 2020: 3581–3585.
- 23 Cayce JM, Friedman RM, Jansen ED, Mahavaden-Jansen A, Roe AW. 2011. Pulsed infrared light alters neural activity in rat somatosensory cortex in vivo. *Neuroimage*. 57:155–166.
- 24 Cayce JM, et al. 2014. Infrared neural stimulation of primary visual cortex in non-human primates. *Neuroimage*. 84:181–190.
- 25 Matic AI, Walsh JT, Richter C-P. 2011. Spatial extent of cochlear infrared neural stimulation determined by tone-on-light masking. *J Biomed Opt*. 16:118002.
- 26 Wells J, Konrad P, Kao C, Jansen ED, Mahadevan-Jansen A. 2007. Pulsed laser versus electrical energy for peripheral nerve stimulation. *J Neurosci Methods*. 163:326–337.
- 27 Boyden ES, Zhang F, Bamberg E, Nagel G, Deisseroth K. 2005. Millisecond-timescale, genetically targeted optical control of neural activity. *Nat Neurosci*. 8:1263–1268.
- 28 Liu X, et al. 2021. Nonthermal and reversible control of neuronal signaling and behavior by midinfrared stimulation. *Proc Natl Acad Sci U S A*. 118:e2015685118.
- 29 Chernov MM, Chen G, Roe AW. 2014. Histological assessment of thermal damage in the brain following infrared neural stimulation. *Brain Stimul*. 7:476–482.
- 30 Wells JD, et al. 2007. Optically mediated nerve stimulation: identification of injury thresholds. *Lasers Surg Med*. 39:513–526.
- 31 Goyal V, Rajguru S, Matic AI, Stock SR, Richter C-P. 2012. Acute damage threshold for infrared neural stimulation of the cochlea: functional and histological evaluation. *Anat Record (Hoboken)*. 295:1987–1999.
- 32 Cayce JM, et al. 2015. Infrared neural stimulation of human spinal nerve roots in vivo. *Neurophotonics*. 2:015007.
- 33 Benabid AL, et al. 1991. Long-term suppression of tremor by chronic stimulation of the ventral intermediate thalamic nucleus. *Lancet*. 337:403–406.
- 34 Karas PJ, et al. 2019. Deep brain stimulation for obsessive compulsive disorder: evolution of surgical stimulation target parallels changing model of dysfunctional brain circuits. *Front Neurosci*. 12:998.
- 35 Senova S, et al. 2019. Deep brain stimulation for refractory obsessive-compulsive disorder: towards an individualized approach. *Front Psychiatry*. 10:905.
- 36 Horn A. 2022. Predicting treatment response based on DBS connectivity. In: Horn A, editor. *Connectomic deep brain stimulation*. Cambridge (MA): Academic Press. p. 375–404.
- 37 Mason XL, Cross KA, Arac A, Bordelon Y, Wu AD. 2022. Vim-Thalamic deep brain stimulation for cervical dystonia and upper-limb tremor: quantification by markerless-3D kinematics and accelerometry. *Tremor Other Hyperkinet Mov (N Y)*. 12:5.
- 38 Jakobs M, Fomenko A, Lozano AM, Kiening KL. 2019. Cellular, molecular, and clinical mechanisms of action of deep brain stimulation—a systematic review on established indications and outlook on future developments. *EMBO Mol Med*. 11:e9575.
- 39 Bartlett EL, Coventry BS. 2023. Reinforcement learning based closed-loop neuromodulation system. United States Patent and Trademark Office (USPTO #18/083,490):1–25.
- 40 Coventry BS, Bartlett EL. 2023. Closed-loop reinforcement learning based deep brain stimulation using SpikerNet: A computational model. 2023 11th International IEEE EMBS Conference on Neural Engineering; Baltimore, MD, USA, pp. 1–4.
- 41 Little S, et al. 2013. Adaptive deep brain stimulation in advanced Parkinson disease. *Ann Neurol*. 74:449–457.
- 42 Rosin B, et al. 2011. Closed-Loop deep brain stimulation is superior in ameliorating Parkinsonism. *Neuron*. 72:370–384.
- 43 Little S, Brown P. 2020. Debugging adaptive deep brain stimulation for Parkinson’s disease. *Mov Disord*. 35:555–561.
- 44 Krook-Magnuson E, Gelinas JN, Soltesz I, Buzsáki G. 2015. Neuroelectronics and biooptics: closed-loop technologies in neurological disorders. *JAMA Neurol*. 72:823.
- 45 Smyth C, et al. 2023. Adaptive deep brain stimulation for sleep stage targeting in Parkinson’s disease. *Brain Stimul*. 16:1292–1296.

- 46 Mudry A, Mills M. 2013. The early history of the cochlear implant: a retrospective. *JAMA Otolaryngol Head Neck Surg.* 139:446.
- 47 Behr R, et al. 2014. New outcomes with auditory brainstem implants in NF2 patients. *Otol Neurotol.* 35:1844–1851.
- 48 Lim HH, Lenarz T. 2015. Auditory midbrain implant: research and development towards a second clinical trial. *Hear Res.* 322:212–223.
- 49 Koivuniemi AS, Otto KJ. 2011. Asymmetric versus symmetric pulses for cortical microstimulation. *IEEE Trans Neural Syst Rehabil Eng.* 19:468–476.
- 50 Verner RS, Banks MI, Bartlett EL. 2 November 2017. Global state changes induce non-reciprocal reduction of mutual information in the Thalamocortical network. bioRxiv 213272. <https://doi.org/10.1101/213272>, preprint: not peer reviewed.
- 51 Lim HH, et al. 2007. Electrical stimulation of the midbrain for hearing restoration: insight into the functional organization of the human central auditory system. *J Neurosci.* 27:13541–13551.
- 52 Bartlett EL, Wang X. 2011. Correlation of neural response properties with auditory thalamus subdivisions in the awake marmoset. *J Neurophysiol.* 105:2647–2667.
- 53 Winer JA. 1984. The human medial geniculate body. *Hear Res.* 15:225–247.
- 54 Parthasarathy A, Bartlett E. 2012. Two-channel recording of auditory-evoked potentials to detect age-related deficits in temporal processing. *Hear Res.* 289:52–62.
- 55 Parthasarathy A, Cunningham PA, Bartlett EL. 2010. Age-Related differences in auditory processing as assessed by amplitude-modulation following responses in quiet and in noise. *Front Ag Neurosci.* 2:152.
- 56 Venkataraman Y, Bartlett EL. 2014. Postnatal development of auditory central evoked responses and thalamic cellular properties. *Dev Neurobiol.* 74:541–555.
- 57 Bartlett EL. 2013. The organization and physiology of the auditory thalamus and its role in processing acoustic features important for speech perception. *Brain Lang.* 126:29–48.
- 58 Smith PH, Uhlrich DJ, Manning KA. 2019. Evaluation of medial division of the medial geniculate (MGM) and posterior intralaminar nucleus (PIN) inputs to the rat auditory cortex, amygdala, and striatum. *J Comp Neurol.* 527:1478–1494.
- 59 Aculight-Lockheed Martin. 2011. Class 2 device recall Lockheed martin Aculight Capella R1850 Laser. <https://www.accessdata.fda.gov/scripts/cdrh/cfdocs/cfres/res.cfm?id=96310>.
- 60 Gregory BA, et al. 17 September 2022. Structural and functional changes of pyramidal neurons at the site of an implanted microelectrode array in rat primary motor cortex. bioRxiv 507997. <https://doi.org/10.1101/2022.09.15.507997>, preprint: not peer reviewed.
- 61 Song S, Regan B, Ereifej ES, Chan ER, Capadona JR. 2022. Neuroinflammatory gene expression analysis reveals pathways of interest as potential targets to improve the recording performance of intracortical microelectrodes. *Cells.* 11:2348.
- 62 Liégeois-Chauvel C, Musolino A, Badier JM, Marquis P, Chauvel P. 1994. Evoked potentials recorded from the auditory cortex in man: evaluation and topography of the middle latency components. *Electroencephalogr Clin Neurophysiol.* 92:204–214.
- 63 Musiek F, Nagle S. 2018. The middle latency response: a review of findings in various central nervous system lesions. *J Am Acad Audiol.* 29:855–867.
- 64 Race N, Lai J, Shi R, Bartlett EL. 2017. Differences in postinjury auditory system pathophysiology after mild blast and nonblast acute acoustic trauma. *J Neurophysiol.* 118:782–799.
- 65 Han EX, Fernandez JM, Swanberg C, Shi R, Bartlett EL. 2021. Longitudinal auditory pathophysiology following mild blast-induced trauma. *J Neurophysiol.* 126:1172–1189.
- 66 Sankar V, et al. 2014. Electrode impedance analysis of chronic tungsten microwire neural implants: understanding abiotic vs. biotic contributions. *Front Neuroeng.* 7:13.
- 67 Gerstein GL. 1960. Analysis of firing patterns in single neurons. *Science.* 131:1811–1812.
- 68 Hill MRH, Fried I, Koch C. 2015. Quantification and classification of neuronal responses in kernel-smoothed peristimulus time histograms. *J Neurophysiol.* 113:1260–1274.
- 69 Dimatteo I, Genovese CR, Kass RE. 2001. Bayesian curve-fitting with free-knot splines. *Biometrika.* 88:1055–1071.
- 70 Kass RE, Ventura V, Cai C. 2003. Statistical smoothing of neuronal data. *Network.* 14:5–15.
- 71 Kass RE, Ventura V, Brown EN. 2005. Statistical issues in the analysis of neuronal data. *J Neurophysiol.* 94:8–25.
- 72 Chung Y, Rabe-Hesketh S, Dorie V, Gelman A, Liu J. 2013. A non-degenerate penalized likelihood estimator for variance parameters in multilevel models. *Psychometrika.* 78:685–709.
- 73 Chung Y, Gelman A, Rabe-Hesketh S, Liu J, Dorie V. 2015. Weakly informative prior for point estimation of covariance matrices in hierarchical models. *J Educ Behav Stat.* 40:136–157.
- 74 Gelman A, Hill J. 2006. *Data analysis using regression and multilevel/hierarchical models.* 1st ed. Cambridge: Cambridge University Press.
- 75 Kruschke JK, Vanpaemel W. 2015. Bayesian estimation in hierarchical models. In: Busemeyer JR, Wang Z, Townsend JT, Eidels A, editors. *The Oxford Handbook of Computational and Mathematical Psychology.* Oxford: Oxford University Press. p. 279–299.
- 76 Gelman A. 2006. Prior distributions for variance parameters in hierarchical models (comment on article by Browne and Draper). *Bayesian Anal.* 1:515–534.
- 77 Higgins JPT, Thompson SG, Spiegelhalter DJ. 2009. A Re-evaluation of random-effects meta-analysis. *J R Stat Soc Ser A Stat Soc.* 172:137–159.
- 78 Coventry BS, Bartlett EL. 21 November 2023. Practical Bayesian inference in neuroscience: Or how I learned to stop worrying and embrace the distribution. bioRxiv 567743. <https://doi.org/10.1101/2023.11.19.567743>, preprint: not peer reviewed.
- 79 Strong SP, Koberle R, De Ruyter Van Steveninck RR, Bialek W. 1998. Entropy and information in neural spike trains. *Phys Rev Lett.* 80:197–200.
- 80 Panzeri S, Senatore R, Montemurro MA, Petersen RS. 2007. Correcting for the sampling bias problem in spike train information measures. *J Neurophysiol.* 98:1064–1072.
- 81 Miller LM, Escabi MA, Read HL, Schreiner CE. 2001. Functional convergence of response properties in the auditory thalamocortical system. *Neuron.* 32:151–160.
- 82 Wang X, Lu T, Bendor D, Bartlett E. 2008. Neural coding of temporal information in auditory thalamus and cortex. *Neuroscience.* 154:294–303.
- 83 Vasquez-Lopez SA, et al. 2017. Thalamic input to auditory cortex is locally heterogeneous but globally tonotopic. *eLife.* 6:e25141.
- 84 Profant O, Burianová J, Syka J. 2013. The response properties of neurons in different fields of the auditory cortex in the rat. *Hear Res.* 296:51–59.
- 85 Hentschke H, Raz A, Krause BM, Murphy CA, Banks MI. 2017. Disruption of cortical network activity by the general anaesthetic isoflurane. *Br J Anaesth.* 119:685–696.

- 86 Shiramatsu TI, et al. 2016. Microelectrode mapping of tonotopic, laminar, and field-specific organization of thalamo-cortical pathway in rat. *Neuroscience*. 332:38–52.
- 87 Scherer M, et al. 2022. Single-neuron bursts encode pathological oscillations in subcortical nuclei of patients with Parkinson's disease and essential tremor. *Proc Natl Acad Sci U S A*. 119: e2205881119.
- 88 Cagnan H, Denison T, McIntyre C, Brown P. 2019. Emerging technologies for improved deep brain stimulation. *Nat Biotechnol*. 37:1024–1033.
- 89 Harris KD, Thiele A. 2011. Cortical state and attention. *Nat Rev Neurosci*. 12:509–523.
- 90 Agostinelli F, McAleer S, Shmakov A, Baldi P. 2019. Solving the Rubik's cube with deep reinforcement learning and search. *Nat Mach Intell*. 1:356–363.
- 91 McCaughey RG, Chlebicki C, Wong BJF. 2010. Novel wavelengths for laser nerve stimulation. *Lasers Surg Med*. 42:69–75.
- 92 Izzo AD, et al. 2008. Laser stimulation of auditory neurons: effect of shorter pulse duration and penetration depth. *Biophys J*. 94: 3159–3166.
- 93 Duke AR, et al. 2013. Transient and selective suppression of neural activity with infrared light. *Sci Rep*. 3:2600.
- 94 Duke AR, Lu H, Jenkins MW, Chiel HJ, Jansen ED. 2012. Spatial and temporal variability in response to hybrid electro-optical stimulation. *J Neural Eng*. 9:036003.
- 95 Ford JB, et al. 2021. Optimizing thermal block length during infrared neural inhibition to minimize temperature thresholds. *J Neural Eng*. 18:056016.
- 96 Wang M, et al. 2020. Prolonged post-stimulation response induced by 980-nm infrared neural stimulation in the rat primary motor cortex. *Lasers Med Sci*. 35:365–372.
- 97 Smith PH, Uhlrich DJ, Manning KA, Banks MI. 2012. Thalamocortical projections to rat auditory cortex from the ventral and dorsal divisions of the medial geniculate nucleus. *J Comp Neurol*. 520:34–51.
- 98 Wang X, Lu T, Snider RK, Liang L. 2005. Sustained firing in auditory cortex evoked by preferred stimuli. *Nature*. 435:341–346.
- 99 Rutkowski RG, Shackleton TM, Schnupp JWH, Wallace MN, Palmer AR. 2002. Spectrotemporal receptive field properties of single units in the primary, dorsocaudal and ventrorostral auditory cortex of the guinea pig. *Audiol Neurotol*. 7:214–227.
- 100 Polley DB, Read HL, Storage DA, Merzenich MM. 2007. Multiparametric auditory receptive field organization across five cortical fields in the albino rat. *J Neurophysiol*. 97:3621–3638.
- 101 Ranasinghe KG, Vrana WA, Matney CJ, Kilgard MP. 2013. Increasing diversity of neural responses to speech sounds across the central auditory pathway. *Neuroscience*. 252:80–97.
- 102 Bartlett EL, Wang X. 2007. Neural representations of temporally modulated signals in the auditory thalamus of awake primates. *J Neurophysiol*. 97:1005–1017.
- 103 Baker KB, Montgomery EB, Rezai AR, Burgess R, Lüders HO. 2002. Subthalamic nucleus deep brain stimulus evoked potentials: physiological and therapeutic implications: evoked potentials from STN DBS. *Mov Disord*. 17:969–983.
- 104 Cayce JM, et al. 2014. Calcium imaging of infrared-stimulated activity in rodent brain. *Cell Calcium*. 55:183–190.
- 105 Winer JA, Larue DT. 1987. Patterns of reciprocity in auditory thalamocortical and corticothalamic connections: study with horseradish peroxidase and autoradiographic methods in the rat medial geniculate body. *J Comp Neurol*. 257:282–315.
- 106 Zhang Y, Suga N. 2000. Modulation of responses and frequency tuning of thalamic and collicular neurons by cortical activation in mustached bats. *J Neurophysiol*. 84:325–333.
- 107 Pan L, et al. 2023. Infrared neural stimulation in human cerebral cortex. *Brain Stimul*. 16:418–430.
- 108 Meneghetti M, et al. 2023. Soft monolithic infrared neural interface for simultaneous neurostimulation and electrophysiology. *Light Sci Appl*. 12:127.
- 109 Jacques SL. 1992. Laser-Tissue interactions: photochemical, photothermal, and photomechanical. *Surg Clin North Am*. 72: 531–558.
- 110 Matic AI, et al. 2013. Behavioral and electrophysiological responses evoked by chronic infrared neural stimulation of the cochlea. *PLoS One*. 8:e58189.
- 111 Rabbitt RD, et al. 2016. Heat pulse excitability of vestibular hair cells and afferent neurons. *J Neurophysiol*. 116:825–843.
- 112 Wells J, et al. 2007. Biophysical mechanisms of transient optical stimulation of peripheral nerve. *Biophys J*. 93:2567–2580.
- 113 Shapiro MG, Richter C-P, Homma K, Villarreal S, Bezanilla F. 2012. Infrared light excites cells by changing their electrical capacitance. *Nat Commun*. 3:736.
- 114 Beier HT, Tolstykh GP, Musick JD, Thomas RJ, Ibey BL. 2014. Plasma membrane nanoporation as a possible mechanism behind infrared excitation of cells. *J Neural Eng*. 11:066006.
- 115 Lumbreras V, Bas E, Gupta C, Rajguru SM. 2014. Pulsed infrared radiation excites cultured neonatal spiral and vestibular ganglion neurons by modulating mitochondrial calcium cycling. *J Neurophysiol*. 112:1246–1255.
- 116 Tolstykh GP, Olsovsky CA, Ibey BL, Beier HT. 2017. Ryanodine and IP 3 receptor-mediated calcium signaling play a pivotal role in neurological infrared laser modulation. *Neurophotonics*. 4:025001.
- 117 Ganguly M, et al. 2019. Voltage-gated potassium channels are critical for infrared inhibition of action potentials: an experimental study. *Neurophotonics*. 6:040501.
- 118 Little S, et al. 2016. Adaptive deep brain stimulation for Parkinson's disease demonstrates reduced speech side effects compared to conventional stimulation in the acute setting. *J Neurol Neurosurg Psychiatry*. 87:1388–1389.
- 119 Guo W, Wu X, Khan U, Xing X. 2021. EDGE: explaining deep reinforcement learning policies. 35th Conference on Neural Information Processing Systems (NeurIPS, 2021); pp. 12222–12236.
- 120 Okun MS, et al. 2005. Management of referred deep brain stimulation failures: a retrospective analysis from 2 movement disorders centers. *Arch Neurol*. 62:1250.
- 121 Gage GJ, et al. 2012. Surgical implantation of chronic neural electrodes for recording single unit activity and electrocorticographic signals. *J Vis Exp*. 3565.
- 122 Lamas V, Estévez S, Pernía M, Plaza I, Merchán MA. 2017. Stereotactically-guided ablation of the rat auditory cortex, and localization of the lesion in the brain. *J Vis Exp*. 56429.
- 123 Christianson GB, Sahani M, Linden JF. 2011. Depth-Dependent temporal response properties in core auditory cortex. *J Neurosci*. 31:12837–12848.
- 124 Thompson AC, et al. 2015. Infrared neural stimulation fails to evoke neural activity in the deaf guinea pig cochlea. *Hear Res*. 324:46–53.
- 125 Teudt IU, Maier H, Richter CP, Kral A. 2011. Acoustic events and "optophonic" cochlear responses induced by pulsed near-infrared LASER. *IEEE Trans Biomed Eng*. 58:1648–1655.

- 126 Ter-Mikaelian M, Sanes DH, Semple MN. 2007. Transformation of temporal properties between auditory midbrain and cortex in the awake Mongolian gerbil. *J Neurosci*. 27:6091–6102.
- 127 Quiroga RQ, Nadasdy Z, Ben-Shaul Y. 2004. Unsupervised spike detection and sorting with wavelets and superparamagnetic clustering. *Neural Comput*. 16:1661–1687.
- 128 Krause BM, Raz A, Uhlrich DJ, Smith PH, Banks MI. 2014. Spiking in auditory cortex following thalamic stimulation is dominated by cortical network activity. *Front Syst Neurosci*. 8:170.
- 129 Walker HC, et al. 2012. Short latency activation of cortex by clinically effective thalamic brain stimulation for tremor. *Mov Disord*. 27:1404–1412.
- 130 Gerstein GL, Perkel DH. 1969. Simultaneously recorded trains of action potentials: analysis and functional interpretation. *Science*. 164:828–830.
- 131 Paszke A, et al. 3 December 2019. PyTorch: An imperative style, high-performance deep learning library. arXiv 01703. <https://doi.org/10.48550/arXiv.1912.01703>, preprint: not peer reviewed.
- 132 Mnih V, et al. 2015. Human-level control through deep reinforcement learning. *Nature*. 518:529–533.
- 133 Sutton RS, Barto AG. 2018. *Reinforcement learning*. 2ed. Cambridge (MA): The MIT Press.
- 134 Fujimoto S, van Hoof H, Meger D. 22 October 2018. Addressing function approximation error in actor-critic methods. bioRxiv 09477. <https://doi.org/10.48550/arXiv.1802.09477>, preprint: not peer reviewed.